

Multitechnique investigation of sulfur phases in the corrosion product layers of iron corroded in long-term anoxic conditions: From micrometer to nanometer scale

Muriel Bouttemy¹  | Sophie Grousset^{2,3,4} | Florence Mercier-Bion² | Delphine Neff² | Arnaud Etcheberry¹ | Philippe Dillmann²

¹ILV, Université de Versailles Saint-Quentin en Yvelines, Université Paris-Saclay, 78035 Versailles, France

²LAPA-IRAMAT, NIMBE, CEA, CNRS, Université Paris-Saclay, CEA Saclay, 91191 Gif-sur-Yvette, France

³IRSN, PRP-DGE/SRTG/LETIS, B.P. 17, 92262 Fontenay aux Roses Cedex, France

⁴Andra, Direction de la recherche et développement, 1-7 rue Jean-Monnet, 92298 Châtenay-Malabry Cedex, France

Correspondence

Muriel Bouttemy, ILV, Université de Versailles Saint-Quentin en Yvelines, Université Paris-Saclay, 78035 Versailles, France.
Email: muriel.bouttemy@uvsq.fr

Florence Mercier-Bion, LAPA-IRAMAT, NIMBE, CEA, CNRS, Université Paris-Saclay, CEA Saclay, 91191 Gif-sur-Yvette, France.
Email: florence.mercier@cea.fr

Funding information

Agence nationale pour la gestion des déchets radioactifs (Andra); Institut de Radioprotection et de Sécurité Nucléaire (IRSN)

The understanding of anoxic corrosion mechanism is essential to develop predictive models targeting to optimize extraction and conservation operations as well as aging behavior of industrial or cultural heritage ferrous objects. The corrosion product layers issued from carbonated anoxic environment of iron often contain iron sulfides, as pyrite FeS₂, greigite Fe₃S₄, and mackinawite FeS, mixed at the submicron scale, and their presence strongly impacts the corrosion processes. The determination of their spatial arrangement in corrosion product layer directly informs about their origin (bacterial or inorganic) and, so, about the corrosion mechanisms. Previous studies have displayed that sulfur isotopic measurements using nano-Secondary Ion Mass Spectrometry (SIMS) are particularly relevant to discriminate between biotic or abiotic origin of iron sulfides. But this technique does not enable to correlate this origin to the nature of sulfide compounds. In this work, an innovative approach combining μ -Raman spectroscopy (structural identification) for sulfide compounds localization at micrometric scale and nano-Auger spectroscopy (chemical diagnostic) at higher spatial resolution is presented. This multi-technique methodology is detailed and its capabilities evaluated on an archeological system. Auger spectra of pure iron sulfides phases (pyrite, greigite, and mackinawite) are obtained and, by considering the derivative spectra of Fe-MVV and of S-LVV spectral regions, evidence-specific signatures for each phase, and so, the possibility to differentiate them. This result enables to propose a complete determination of the iron sulfides mix by coupling nano-SIMS and nano-Auger to get a complete knowledge of the role of iron sulfides in the anoxic corrosion of ferrous objects.

KEYWORDS

cultural heritage objects, iron corrosion, iron sulfides, metrology, nano-Auger spectroscopy, μ -Raman spectroscopy

1 | INTRODUCTION

The study of anoxic corrosion process of ferrous metals is a matter of concern for industrial sector (pipelines^{1,2} and metallic containers for nuclear waste storage)³⁻⁵ and also for cultural heritage object conservation.⁶ In addition to iron oxides and carbonates, as magnetite,

siderite, and chukanovite, the recurring identification of iron sulfides in the corrosion product layers (CPLs) in either terrestrial⁷ or marine environments^{7,8} is of particular interest. Although iron sulfides are minor phases and sometimes very localized in iron CPLs, they play a crucial role in the corrosion rates of ferrous objects. Indeed, these conductive phases can cause galvanic corrosion and/or pH

heterogeneities leading to the increase of the corrosion rate of the steel. Conversely, the formation of a homogeneous deposition of iron sulfides constitutes a passive layer that can decrease the corrosion rate.

In natural environment, the presence of microorganisms such as sulfate-reducing bacteria (SRB) may foster the precipitation of iron sulfide phases by transforming sulfates into sulfides.^{1,2,9,10} Moreover, there are not only biotic but also abiotic sources of sulfides like the sulfide minerals, as pyrite, present in the environment. The aqueous dissolution of iron metal into ferrous ions associated with the presence of sulfides, biotic or abiotic one, must lead to iron sulfides precipitation in the CPL.

In previous papers,^{7,8} the characterization of the CPL of anoxic ferrous archaeological nails by μ -Raman spectroscopy has evidenced that different iron sulfides, as greigite (Fe_3S_4) and crystalline mackinawite (FeS), are mixed at the submicrometric scale in a corrosion layer mainly constituted of iron carbonates. A variable proportion of greigite and crystalline mackinawite phases in different locations of the CPL was observed, pointing out the need to solve this "intimate mix" at higher spatial resolution to take account for those fluctuations and be as closely as possible to the real system.

Indeed, this spatial distribution of sulfide compounds directly results from the corrosion process, and so, conveys crucial information to anticipate the degradation of ferrous objects during extraction, storage, or conservation operations. In addition, understanding the formation mechanisms of these different iron sulfides, and particularly if they come from a bacterial origin or if they are formed by an inorganic process, is an important challenge. Recent studies have demonstrated the contribution of nano-SIMS to this problematic. Indeed, the sulfur isotopic determination on iron corroded in anoxic condition, in the absence or in the presence of SRB, has showed that it was possible to distinguish the origin of the iron sulfides.¹¹ Depletion in ^{34}S was observed in iron sulfides formed with the action of SRB whereas an increase in ^{34}S was evidenced for iron sulfides corroded without SRB. Indeed, for their sulfato-reduction metabolism, SRB preferentially uses the lighter sulfur isotope ^{32}S leaving the medium enriched in the heavier sulfur isotope ^{34}S .¹² H_2S formed during the bacterial sulfate reduction is then depleted in ^{34}S whereas the remaining sulfate is enriched in ^{34}S .¹³ However, if crucial information is obtained by nano-SIMS, this technique cannot give chemical information.

Recent studies, mainly on conductor and semiconductor materials, have demonstrated the capabilities of new generation Auger nano-probes to reach high spatial resolution (approximately 10 nm ultimate resolution) and to identify chemical environments (relative energy resolution dE/E until 0.06%), making this technique relevant at first sight for a suitable submicrometric separation of different chemical phases.^{14,15} However, it is noteworthy that the literature concerning the Auger investigation of iron sulfides is rare and was published some 10 years ago. As an example, Lee and Montano¹⁶ used Auger spectroscopy to study different iron sulfide surfaces (FeS_2 , Fe_7S_8 , and FeS), but this study revealed that only FeS could be separated from the appearance of 2 additional features on the derived $\text{Fe-M}_{2,3}\text{VV}$ signal.

First part of the present work was then dedicated to the acquisition of standard Auger spectra of the different iron sulfides

representative of those evidenced in CPL layers of iron objects issued from anoxic environment^{7,8}: mackinawite, greigite, and pyrite. Both Fe-MVV and S-LVV low kinetic energy Auger transitions, presenting higher sensitivity to changes in the chemical environment, and so, probable specific fingerprints, were considered. The feasibility of Scanning Auger Microscopy (SAM) was then evaluated on an archeological nail.

2 | MATERIALS AND METHODS

2.1 | Samples

Three iron sulfur phases representative of the main phases observed in iron CPL issued from anoxic environment, mackinawite FeS , greigite Fe_3S_4 , and pyrite FeS_2 , were considered in this work and analyzed by nano-Auger for the determination of their Auger spectral fingerprints and the constitution of a data basis for this type of compounds.

In the former studies on iron sulfides,^{17,18} mackinawite was considered as a metastable sulfur-deficient iron(II) sulfide but more recently some authors have showed that its formula is rather FeS .^{19,20} The formula and structure of greigite Fe_3S_4 make it the sulfide equivalent of magnetite Fe_3O_4 with the mix of Fe(II) and Fe(III) in its crystalline structure. Iron sulfides as mackinawite and greigite have a great reactivity in the presence of O_2 especially if they are freshly synthesized or if they are formed during short-term iron corrosion experiments.²¹ Therefore, mackinawite and greigite are difficult to maintain in their initial state. For this reason, mackinawite FeS_{1-x} , greigite Fe_3S_4 , and pyrite FeS_2 were selected in a natural CPL of ferrous archaeological samples buried in anoxic environment and containing these pure phases.

For pure pyrite and pure mackinawite, the archaeological sample corresponds to a ferrous nail "T6FI2CL3" found in the wood of a Gallo-Roman shipwreck of first century AD buried in anoxic subaquatic site "Arles-Rhone 3." For pure greigite, the archaeological sample corresponds to a ferrous nail "RH12-03" dated of the seventeenth century and issued from a terrestrial site "Raadhuspladsen" at Copenhagen in Denmark.²² The excavation of these nails was carried out in 2008 to 2012 for the site Arles-Rhône 3 and in 2012 for that of Raadhuspladsen.⁷

As these phases are present in areas of few tenths micrometers dimensions, they were carefully localized, thanks to μ -Raman spectroscopy analyses (see below) assessing that in the reference zones, the compounds are pure at the scale of the analyzed volume.

The 2 archaeological nails were prepared in N_2 atmosphere to be compatible for both μ -Raman spectroscopy and nano-Auger experiments. They were embedded with epoxy resin (Specifix-20, Struers®) and cut in circular sections of 10 mm diameter and 1 mm thickness. Then they were polished in ethanol, to avoid their dissolution, down to grad 4000 with SiC paper and to 1 μm diamond preparation. The electron-induced Auger process, by nature, is more favorable for metals and semiconductors materials analysis,¹³ but because of the semiconductive properties of iron sulfides, the sample preparation did not require specific preparation to overcome huge charging effects.

2.2 | Analytical techniques

2.2.1 | μ -Raman spectroscopy

μ -Raman spectroscopy measurements were carried out via an Invia Reflex[®] spectrometer with an excitation wavelength of 532 nm. The laser power was filtered down to 0.1 mW, and the spectra were recorded with a resolution of 2 cm^{-1} . The beam diameter was about 1 μm , as well as the probed depth ensuring the homogeneity of the selected zone, larger than the Auger probe. The spectrometer calibration was obtained from a silicon wafer using the main peak at 520.5 cm^{-1} . Acquisition and treatment of the spectra were obtained with the software Wire 3.4[®]. The spectra are presented without smoothing or line fitting. The recorded spectra were compared with the spectra obtained on the corresponding phases.^{7,8}

2.2.2 | Nano-Auger electron spectroscopy

Auger electron escape depth being inferior to 5 nm, the samples surface was cleaned prior to analysis by a short Ar^+ ionic bombardment (almost 1 mm^2). Nano-Auger characterizations were performed with a JEOL JAMP 9500F nano-probe equipped with a patented "in-lens" Schottky field emission gun and a hemispherical analyzer. The ultimate resolutions delivered for this equipment on the surface are 3 nm (25 kV, 10 pA) for scanning electron microscopy and 8 nm (25 kV, 1 nA) for Auger electron spectroscopy. Thus, the analyzed volume with the Auger electron spectroscopy is largely smaller than the Raman one (see above).

Experiments were carried out at 15 kV, 5 to 40 nA, tilt 40° and defocused spots to limit charging effect and increase the signal-to-

noise ratio (with respect to the collection angle geometry). Therefore, no charge compensation was needed, avoiding misshapen spectra observation (mainly peaks enlargement) and artificial energy position drift. The kinetic energy scale was calibrated with reference to the residual carbon Auger signal (arising from superficial contamination layer) positioned at 263 eV in direct acquisition mode of the Auger spectrum $N(E) = \text{intensity distribution (counts) vs kinetic energy (eV)}$. For the Fe-MVV (17-80 eV) and S-LVV (120-170 eV) spectral regions, high energy resolution mode was selected ($dE/E = 0.15\%$), favoring chemical sensitivity but to the detriment of signal intensities. Auger wide scan spectra (0-2250 eV) were also acquired to determine the C, O, Fe, and S contents to certify the positioning at local scale and the nature of the sulfide compounds.

3 | RESULTS

3.1 | μ -Raman analyses on pure iron sulfides phases

Figure 1 presents optical images of the CPL in transverse section of the archaeological ferrous nails "T6FI2CL3" (a, b) and "RH12-03" (c) and the μ -Raman spectra of their pure phases of iron sulfides (d-f).

In the CPL of "T6FI2CL3," the bright golden zones (a) correspond to the presence of pure pyrite FeS_2 as evidenced by the 3 Raman signals at 348, 383, and 432 cm^{-1} (d). The mat golden areas shown on the optical image (b) are associated with pure mackinawite, as confirmed by the μ -Raman spectrum (e) presenting a predominant band at 296 cm^{-1} attributed to Fe(II)-S stretching modes.^{7,21}

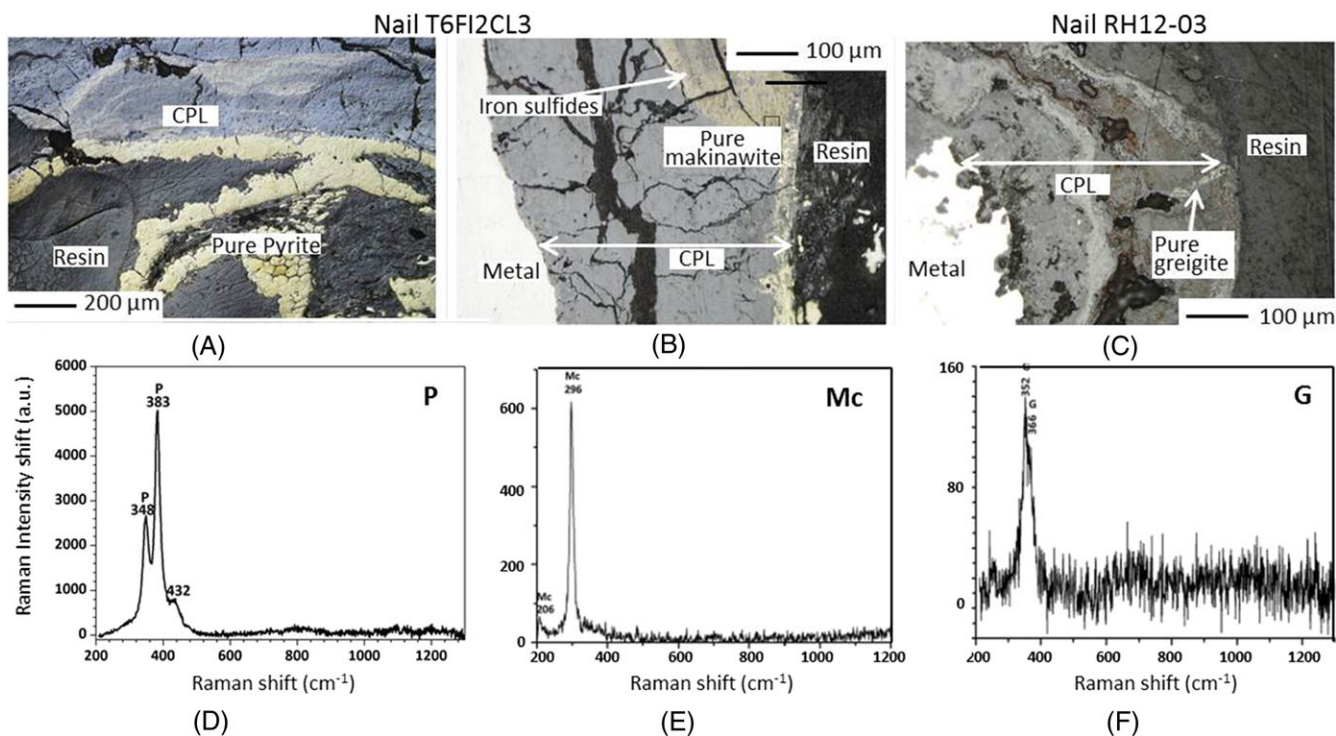


FIGURE 1 Ferrous nail "T6FI2CL3," A, B, optical images of the corrosion product layer (CPL) in transverse section; ferrous nail "RH12-03," C, optical image of the CPL in transverse section; D, E, μ -Raman spectra of the pure pyrite FeS_2 (P) and of the pure mackinawite (Mc) in "T6FI2CL3"; F, μ -Raman spectrum of the pure greigite (G) in "RH12-03"

In the CPL of "RH12-03," the mat golden strip shown on the optical image (c) corresponds to pure greigite Fe_3S_4 well characterized by its 2 narrow Raman bands (f) at 350 and 365 cm^{-1} .²¹

3.2 | Nano-Auger analyses on iron sulfide phases

Thanks to μ -Raman analyses, specific location of the 3 pure iron sulfides phases could be identified and easily relocated on secondary electron (SE) images, monitored on the nano-Auger equipment. Moreover, the nature of the sulfide phase was certified prior high energy resolution spectra acquisition by the determination of the Auger composition obtained on wide scan analyses (not presented here).

3.3 | Auger signals Fe-MVV and S-LVV of pure iron sulfides phases

Figure 2A compares the derivative signal $-d(N(E))/dE$ of the Fe-MVV Auger transition acquired for pyrite, mackinawite, and greigite. The 3 spectra present well-distinct features.

Firstly, from qualitative considerations, a marked shoulder in the energy range (28–34 eV) (named (I)) is observed on the pyrite spectrum, which is weaker for mackinawite and absent for greigite. Secondly, the

negative peak named (II) around 44.0 eV shows different energy positions with the sulfide nature: 43.4 eV for greigite, 44.0 eV for mackinawite, and 45.8 eV for pyrite. Contrarily, the third feature named (III) appears to have a constant energy position. Each of the 3 Fe-MVV spectra presents a different shape especially with regard to the relative preponderance of (II) and (III) peaks. For example, in the case of greigite, the intensities of the 2 contributions are equivalent. To take into account this particularity, which can be considered as a discrimination criteria, the intensity difference in absolute value is measured and mentioned on Figure 2A (Δ values).

On the other hand, derivative signals of the S-LVV Auger transitions of the 3 iron sulfides were also compared Figure 2B. At the first derivative order, no significant evolution of the peak shape could be evidenced, but differences were visible from the second derivative signal (Figure 2B). The position of the positive right shoulder of the signal (named IV) differs with the nature of the sulfide phase. For mackinawite, the position of the extremum is at 153.4 eV while it is at 154.4 eV for pyrite and at 155.5 eV for greigite: The 3 iron sulfides can be discernable by the S-LVV second derivative signal.

To conclude this part, from the derivative treatment of Auger signals Fe-MVV (in first derivative mode) and of S-LVV (in second derivative mode), mackinawite, greigite, and pyrite can be discriminated.

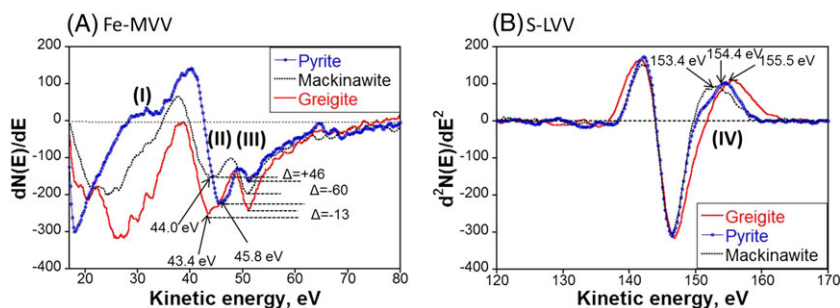


FIGURE 2 Comparison of the derivative signal A, $d(N(E))/dE$ of the Fe-MVV Auger transitions; B, $d^2(N(E))/dE^2$ of the S-LVV Auger transitions for pyrite, mackinawite, and greigite

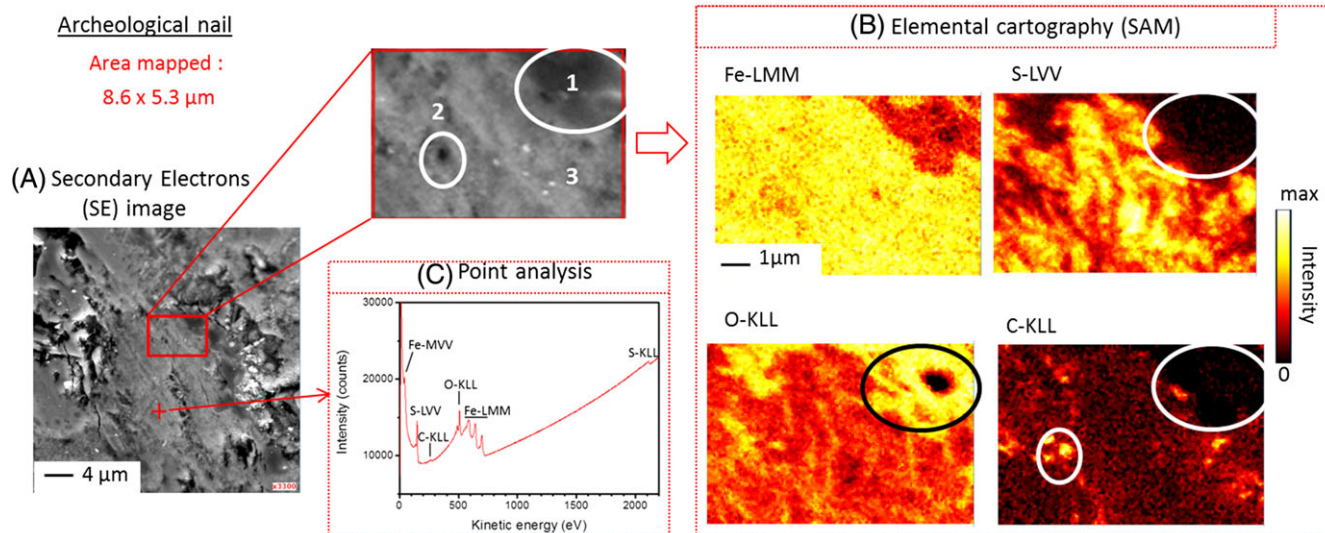


FIGURE 3 A, SE image of the area of interest in the corrosion product layer of "RH12-03," the area scanned, and B, the corresponding Auger elemental maps using carbon C-KLL (263 eV), oxygen O-KLL (503 eV), sulfur S-LVV (146 eV), and iron Fe-LVV (45 eV) intensities measurements, C, Auger wide scan of the main phase

3.4 | CPL Auger maps of the of an archaeological ferrous nail

Potential of SAM analyses to separate iron phases in CPL is evaluated on the archeological nail "RH12-03." The CPL of ferrous archaeological nails issued from carbonated anoxic media is mainly composed of Fe(II) carbonates as siderite FeCO_3 and chukanovite $\text{Fe}_2(\text{OH})_2\text{CO}_3$ with the locally presence of Fe_3O_4 strips.⁷ All these phases can be mixed with iron sulfides at the submicron scale.

Figure 3A displays the SE image of the area of interest in the CPL of "RH12-03" and the area scanned, whose dimensions is $8.6 \mu\text{m}$ per $5.3 \mu\text{m}$. The corresponding Auger elemental maps are obtained using carbon C-KLL (263 eV), oxygen O-KLL (503 eV), sulfur S-LVV (146 eV), and iron Fe-LVV (45 eV) intensities measurements and show the spatial distribution (Figure 3B) of each element (1 pixel $\sim 20 \text{ nm}$). Fe is detected all over the area scanned, although C, O, and S present specific distributions and evidence the presence of different iron phases. On the top right part (zone 1), where a darkest contrast is visible on the SE image, S and C signals are absent on contrary to O whose signal is higher. This region corresponds then to iron oxide only, single phase is also present in some other isolated parts of the mapped area. The C superficial contamination could not be totally removed by sputtering, mainly because of the roughness of the sample, but nevertheless, the C-KLL map informs about the presence of Fe(II) carbonates. Localized C rich regions are observed (zone 2) and correspond to darkest zone on the SE image. Finally, the main part of the map corresponds to a mixed environment with iron sulfur, magnetite Fe_3O_4 , and Fe(II) carbonates in variable proportion (zone 3). This is confirmed by the point analysis (Figure 3C). When using the SAM mode, the information in each pixel is not independent and so the intensity fluctuations are both due to compositions changes and surface roughness. The conversion from intensity map to composition map is not straightforward and requires converting intensity scale to atomic % one, done by appropriate point analyses, but also subtracting the topography contribution, what is not so automated.

Scanning Auger microscopy was satisfactorily performed to spatially separate different phases (iron sulfides, oxides, and carbonates) present in the CPL of ferrous objects at a local scale and extreme surface sensitivity (5 nm escape depth).

4 | CONCLUSION AND FUTURE WORK

The proof of concept of using nano-Auger to submicrometric resolution of iron phases, and particularly iron sulfide identification, in the frame of anoxic corrosion of ferrous objects is done. Pure iron sulfides mackinawite, greigite, and pyrite were characterized, and specific Auger signatures of high energy resolution Fe-MVV and S-LVV, which had not been previously reported in the literature to our knowledge, were evidenced enabling to discriminate the phases. The implementation of nano-Auger on this iron family of compounds is validated, but additional signal treatments have to be developed to determine the contribution of each iron sulfide in a mix of them as it is often the real case in the CPL. The combination of nano-Auger and

of nano-SIMS of a similar spatial resolution will be considered, as being a relevant coupling to allow getting a better understanding of the formation origin of iron sulfides in the CPL of ferrous objects from anoxic environment.

ACKNOWLEDGEMENTS

The authors are grateful for the scientific and financial support of Institut de Radioprotection et de Sûreté Nucléaire (IRSN) and Agence nationale pour la gestion des déchets radioactifs (Andra).

ORCID

Muriel Bouttemy  <http://orcid.org/0000-0001-5907-2576>

REFERENCES

- Venzlaff H, Enning D, Srinivasan J, et al. Accelerated cathodic reaction in microbial corrosion of iron due to direct electron uptake by sulfate-reducing bacteria. *Corros Sci*. 2013;66:88-96.
- Enning D, Garrelfs J. Corrosion of iron by sulfate-reducing bacteria: new views of an old problem. *Appl Environ Microbiol*. 2014;80(4):1226-1236.
- Schlegel ML, Bataillon C, Brucker F, et al. Corrosion of metal iron in contact with anoxic clay at 90 °C: characterization of the corrosion products after two years of interaction. *Appl Geochem*. 2014;51:1-14.
- Léon Y, Saheb M, Drouet E, et al. Interfacial layer on archaeological mild steel corroded in carbonated anoxic environments studied with coupled micro and nano probes. *Corros Sci*. 2014;88:23-35.
- Léon Y, Dillmann P, Neff D, Schlegel M, Foy E, Dynes JJ. Interfacial layers at a nanometre scale on iron corroded in carbonated anoxic environments. *RSC Adv*. 2017;7(33):20101-20115.
- Matthiesen H. Detecting and quantifying ongoing decay of organic archaeological remains: a discussion of different approaches. *Quat Int*. 2015;368:43-50.
- Grousset S, Bayle M, Dauzères A, et al. Study of iron sulphides in long-term iron corrosion processes: characterisations of archaeological artefacts. *Corros Sci*. 2016;112:264-275.
- Remazeilles C, Saheb M, Neff D, et al. Microbiologically influenced corrosion of archeological artefacts: characterisation of iron(II) sulfides by Raman spectroscopy. *J Raman Spectrosc*. 2010;41(11):1425-1433.
- Marchal R. Rôle des bactéries sulfurogènes dans la corrosion du fer. *Oil Gas Sci Technol - Rev IFP*. 1999;54(5):649-659.
- Videla HA, Herrera LK. Understanding microbial inhibition of corrosion. A comprehensive review. *Int Biodeter Biodegr*. 2009;63(7):896-900.
- Grousset S, Mostefaoui S, Chautard C, et al. Détermination de la bioorigine des sulfures de fer présents dans les systèmes de corrosion anoxiques par analyse de la composition isotopique du soufre en nano-SIMS. *Matér Tech*. 2016;104(5):509.
- Rudnicki MD, Elderfield H, Spiro B. Fractionation of sulfur isotopes during bacterial sulfate reduction in deep ocean sediments at elevated temperatures. *Geochim Cosmochim Acta*. 2001;65(5):777-789.
- Habicht KS, Canfield DE, Rethmeier J. Sulfur isotope fractionation during bacterial reduction and disproportionation of thiosulfate and sulfite. *Geochim Cosmochim Acta*. 1998;62(15):2585-2595.
- Martinez E, Yadav P, Bouttemy M, et al. Scanning Auger microscopy for high lateral and depth elemental sensitivity. *Electron Spectrosc Relat Phenom*. 2013;191:86-91.
- Pruyton M, El Gomati MM. *Scanning Auger, Electron Microscopy*. Chichester: John Wiley & Sons; 2006.
- Lee YC, Montano PA. An Auger and EELS study of iron sulfide (FeS_2 , Fe_7S_8 and FeS) surfaces. *Surf Sci*. 1984;143(2-3):442-468.

17. Vaughan DJ, Craig JR. *Mineral Chemistry of Metal Sulfides*. Cambridge: Cambridge University Press; 1978.
18. Benning LG, Wilkin RT, Barnes HL. Reaction pathways in the Fe-S system below 100°C. *Chem Geol*. 2000;167(1-2):25-51.
19. Rickard D, Griffith A, Oldroyd A, et al. The composition of nanoparticulate mackinawite, tetragonal iron(II) monosulfide. *Chem Geol*. 2006;235(3-4):286-298.
20. Rickard D, Luther GW III. Chemistry of iron sulfides. *Chem Rev*. 2007;107(2):514-562.
21. Bourdoiseau JA, Jeannin M, Rémazeilles C, Sabot R, Refait P. The transformation of mackinawite into greigite studied by Raman spectroscopy. *J Raman Spectrosc*. 2011;42(3):496-504.
22. Dahlström H. New light on the early urbanisation of Copenhagen: with the Metro Cityring excavation at Radhuspladsen (Town Hall Square) as a point of departure. *Dan J Archeol*. 2013;2(2):132-145.

How to cite this article: Bouttemy M, Grousset S, Mercier-Bion F, Neff D, Etcheberry A, Dillmann P. Multitechnique investigation of sulfur phases in the corrosion product layers of iron corroded in long-term anoxic conditions: From micrometer to nanometer scale. *Surf Interface Anal*. 2018;1-6. <https://doi.org/10.1002/sia.6441>